

Research Article: New Research | Sensory and Motor Systems

Prior acoustic trauma alters type II afferent activity in the mouse cochlea

https://doi.org/10.1523/ENEURO.0383-21.2021

Cite as: eNeuro 2021; 10.1523/ENEURO.0383-21.2021

Received: 20 September 2021 Accepted: 23 September 2021

This Early Release article has been peer-reviewed and accepted, but has not been through the composition and copyediting processes. The final version may differ slightly in style or formatting and will contain links to any extended data.

Alerts: Sign up at www.eneuro.org/alerts to receive customized email alerts when the fully formatted version of this article is published.

Copyright © 2021 Nowak et al.

This is an open-access article distributed under the terms of the Creative Commons Attribution 4.0 International license, which permits unrestricted use, distribution and reproduction in any medium provided that the original work is properly attributed.

- TITLE: (50 words max) Prior acoustic trauma alters type II afferent activity in the mouse
 cochlea
 cochlea
 - ABBREVIATED TITLE (50 characters max): Acoustic trauma alters type II cochlear afferents
- AUTHORS: Nathaniel Nowak*, Megan Beers Wood*, Elisabeth Glowatzki, and Paul Albert
 Fuchs
 - Johns Hopkins University School of Medicine, Department of Otolaryngology Head and Neck Surgery, Baltimore, MD, USA, 21205
 - * Indicates equal contribution
- Author Contributions: NN and MBW designed research, performed research, analyzed data, and
 wrote the paper. EG and PAF designed research and wrote the paper.
- 13

5

8

9

10

CORRESPONDING AUTHORS: Nathaniel Nowak, <u>nnowak2@jhmi.edu</u>; Megan Beers Wood
 <u>lwood20@jhmi.edu</u>

- 17 Number of Pages: 51
- 18 Number of Figures: 9
- 19 Number of Tables: 4
- 20 Number of Multimedia Files (Videos): 3 21
- 22 Number of Words Abstract- 243
- 23 Number of Words Significance Statement 113
- 24 Number of Words Introduction 547
- 25 Number of Words Discussion 1533
- 26 27
- 28 ACKNOWLEDGEMENTS
- 29 Supported by NIDCD R01 DC016559 (PAF and EG) and R01 DC006476 (EG), T32 DC000023
- 30 (NN and MBW), the Rubenstein Fund for Hearing Research, the George Nager Research
- 31 Professorship (EG) and the David M. Rubenstein Research Professorship (PAF). With thanks to
- 32 Michele Pucak in the Solomon H. Snyder Department of Neuroscience Multiphoton Imaging
- 33 Core, supported by NINDS P30NS050274. With thanks to the laboratory of Dwight Bergles for
- 34 technical assistance and sharing of lab space. With thanks to A. Nyati for assistance with image
- 35 analysis.
- 36 CONFLICT OF INTEREST STATEMENT
- 37 The authors declare no conflict of interest.

38 ABSTRACT (243/250 Words)

39 40 Auditory stimuli travel from the cochlea to the brainstem through type I and type II cochlear 41 afferents. While type I afferents convey information about the frequency, intensity, and timing of 42 sounds, the role of type II afferents remains unresolved. Limited recordings of type II afferents 43 from cochlear apex of pre-hearing rats reveal they are activated by widespread outer hair cell 44 stimulation, ATP, and by the rupture of nearby outer hair cells. Altogether, these lines of 45 evidence suggest that type II afferents sense loud, potentially damaging levels of sound. To 46 explore this hypothesis further, calcium imaging was used to determine the impact of acoustic 47 trauma on the activity of type II cochlear afferents of young adult mice of both sexes. Two 48 known marker genes (*Th*, *Drd2*) and one new marker gene (*Tac1*), expressed in type II afferents 49 and some other cochlear cell types, drove GCaMP6f expression to reveal calcium transients in 50 response to focal damage in the organ of Corti in all turns of the cochlea. Mature type II 51 afferents responded to acute photoablation damage less often but at greater length compared to 52 pre-hearing neurons. In addition, days after acoustic trauma, acute photoablation triggered a 53 novel response pattern in type II afferents and surrounding epithelial cells, delayed bursts of 54 activity occurring minutes after the initial response subsided. Overall, calcium imaging can 55 report type II afferent responses to damage even in mature and noise-exposed animals and 56 reveals previously unknown tissue hyperactivity subsequent to acoustic trauma.

- 57
- 58
- 59
- 60
- 61

62 SIGNIFICANCE STATEMENT (120 words max)

02	SIGNIFICATOL STATEMENT (120 words max)
63	The function of type II cochlear afferents is currently unknown. The prevailing hypothesis is that
64	these neurons detect excessively loud sound and tissue damage within the cochlea. However, this
65	hypothesis has not been directly investigated in fully hearing, mature animals. To this end, we
66	show that type II afferents in mature mice experience prolonged calcium transients in response to
67	focal tissue damage as compared to young, pre-hearing mice. Previous traumatic noise exposure
68	caused novel delayed response patterns. Together, our data support the role of type II cochlear
69	afferents as tissue damage detectors in the cochlea and suggest that changes in type II afferent
70	activity may contribute to pathologies resulting from traumatic noise exposure.
71	
72	
73	
74	
75	
76	
77	
78	
79	
80	
81	
82	
83	
84	

85 INTRODUCTION

86	The spiral ganglion neurons (SGNs) of the cochlea are divided into type I afferents that
87	sensitively encode sound intensity, timing, and frequency, and type II afferents that respond only
88	to loud, broadband sound (Brown, 1994; Flores, Duggan, et al., 2015; Robertson, 1984;
89	Robertson et al., 1999, Weisz et al., 2021). Type I afferents constitute 90-95% of all SGNs, with
90	type II afferents making up the remaining 5% (Perkins and Morest, 1975; Berglund et al., 1987).
91	The two types of SGNs differ not only in proportion but also in innervation pattern as illustrated
92	in Figure 1H-I. Each myelinated type I afferent synapses with one inner hair cell (IHC) and each
93	IHC is contacted by 10-30 unbranched type I afferent dendrites (Liberman, 1982). The small,
94	unmyelinated type II afferents make a 90 degree turn at the level of the OHCs and then extend a
95	long dendritic arbor toward the cochlear base, contacting an average of 24 OHCs (range 9 to
96	100) (Martinez-Monedero et al., 2016; Smith, 1975; Kiang et al., 1982; Berglund and Ryugo,
97	1987; Weisz et al., 2012; Ghimire and Deans, 2019).
97 98	1987; Weisz et al., 2012; Ghimire and Deans, 2019). It has been difficult to determine the function of type II afferents. <i>In vivo</i>
98	It has been difficult to determine the function of type II afferents. In vivo
98 99	It has been difficult to determine the function of type II afferents. <i>In vivo</i> electrophysiological recordings are rare due to the scarcity and small caliber of type II axons
98 99 100	It has been difficult to determine the function of type II afferents. <i>In vivo</i> electrophysiological recordings are rare due to the scarcity and small caliber of type II axons (Brown, 1994; Robertson et al., 1999). Of the limited recordings of putative type II afferents
98 99 100 101	It has been difficult to determine the function of type II afferents. <i>In vivo</i> electrophysiological recordings are rare due to the scarcity and small caliber of type II axons (Brown, 1994; Robertson et al., 1999). Of the limited recordings of putative type II afferents within the eighth nerve, only one had a response to loud, broadband sound (Robertson, 1984;
98 99 100 101 102	It has been difficult to determine the function of type II afferents. <i>In vivo</i> electrophysiological recordings are rare due to the scarcity and small caliber of type II axons (Brown, 1994; Robertson et al., 1999). Of the limited recordings of putative type II afferents within the eighth nerve, only one had a response to loud, broadband sound (Robertson, 1984; Brown, 1994). In a mouse model where type I signaling from IHCs was interrupted, type II
 98 99 100 101 102 103 	It has been difficult to determine the function of type II afferents. <i>In vivo</i> electrophysiological recordings are rare due to the scarcity and small caliber of type II axons (Brown, 1994; Robertson et al., 1999). Of the limited recordings of putative type II afferents within the eighth nerve, only one had a response to loud, broadband sound (Robertson, 1984; Brown, 1994). In a mouse model where type I signaling from IHCs was interrupted, type II afferents were shown to respond only to excessively loud sound (Flores et al., 2015) though see
 98 99 100 101 102 103 104 	It has been difficult to determine the function of type II afferents. <i>In vivo</i> electrophysiological recordings are rare due to the scarcity and small caliber of type II axons (Brown, 1994; Robertson et al., 1999). Of the limited recordings of putative type II afferents within the eighth nerve, only one had a response to loud, broadband sound (Robertson, 1984; Brown, 1994). In a mouse model where type I signaling from IHCs was interrupted, type II afferents were shown to respond only to excessively loud sound (Flores et al., 2015) though see (Weisz et al., 2021). Intracellular recording in apical cochlear segments from pre-hearing

2015), presumably from supporting cells (Gale et al., 2004; Lahne and Gale, 2008, 2010). The
emerging hypothesis is that acoustic trauma activates type II cochlear afferents directly and
through interactions with surrounding epithelia, by analogy with cutaneous nociception (Talagas
et al., 2020).

112 Thus, type II afferents may function as auditory nociceptors. However, the stimuli that 113 drive type II afferents in mature, hearing animals have not been elucidated. In addition, previous 114 cellular studies have been limited to tissues excised from the more accessible apical turn of the 115 cochlea. Damage in the mature cochlea, such as OHC loss due to acoustic trauma, can cause 116 ATP- mediated calcium waves propagated through supporting cells (Anselmi et al., 2008; Gale 117 et al., 2004; Sirko et al., 2019) similar to those occurring within Kölliker's organ during 118 development (Tritsch et al., 2007; Tritsch and Bergles, 2010). The present work presents calcium 119 imaging of type II afferent responses to acute trauma in all turns of the pre-hearing and mature 120 cochlea. In all conditions, type II afferents retain the ability to respond to focal ablation but less 121 reliably in mature cochleas. Additionally, a new mouse model links this activation of type II 122 afferents to calcium waves in epithelial cells. Significantly, the responses of type II afferents and 123 surrounding epithelia to focal ablation are enhanced after noise-induced hearing loss.

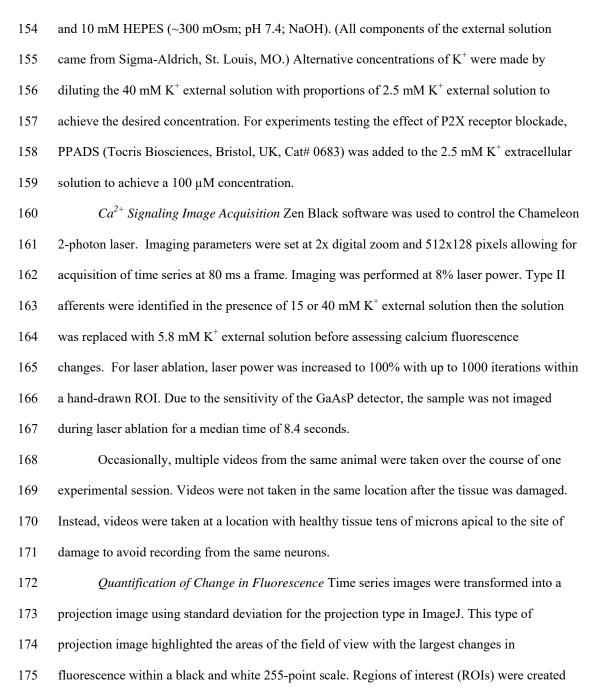
124

125 MATERIALS AND METHODS

- 126 Mice Five mouse models were used in these studies (Table 1). $Th^{2A-CreER}$ and $Drd2^{Cre}$
- 127 homozygous mouse lines were backcrossed to the C57BL/6J strain and maintained
- 128 independently. F1 offspring of either sex of $Th^{2A-CreER}$, $Drd2^{Cre}$, or $Tac1^{Cre}$ bred with
- 129 homozygous GCaMP6f^{fl/fl} mice were generated for the experiments in this paper (Table 1).
- 130 Tamoxifen (Sigma-Aldrich, St. Louis, MO, Catalog number: T5648) was administered by

131	gavage at P3-4 for the Th ^{2A-CreER} ;GCaMP6f animals at a dosage of 0.2 mg in corn oil (Sigma-
132	Aldrich, St. Louis, MO, Cat# C8267). Pre-hearing animals were defined as postnatal 6-10 days
133	of age (Liu et al., 2015). Mature mice were defined as adult mice over 6 weeks and less than 10
134	weeks of age to avoid any confounding effects of accelerated age-related hearing loss associated
135	with the C57BL/6J strain (Johnson et al., 2017; Johnson et al., 1997). Care of the animals
136	followed all institutional guidelines of the Animal Care and Use Committee of JHU SOM.
137	Calcium Imaging Mice were euthanized based on ACME guidelines appropriately for the
138	age of the animal immediately prior to imaging. Pre-hearing animals were placed on a heating
139	pad to maintain core body temperature prior to euthanasia. The otic capsule preparation was
140	adapted from the in situ cochlea preparation described in Sirko and colleagues, wherein the
141	hemi-dissected head was placed in 2.5 mM K^+ external solution on ice and the otic capsule
142	excised from the temporal bone (Sirko et al., 2019). Then, the bone overlying the cochlear
143	epithelium was removed. The fenestrated otic capsule cochlea was mounted on utility wax for
144	observation at room temperature. A gravity perfusion system was constructed on a motorized
145	stage of a 710 LSM Zeiss microscope with a GaAsP detector (Zeiss, Oberkochen, Germany) and
146	Chameleon 2-photon laser (Coherent, Santa Clara, CA). The preparation was placed in external
147	solution and imaged using a 20x non-coverslip-corrected water-immersion objective (Nikon,
148	Inc., Melville, NY). With an objective in place, the 2-photon laser measured 299 mW at 100%
149	power when set to the 920 nm wavelength used in these experiments.
150	Solutions for Bath Application 2.5 mM K^+ external solution was composed of 2.5 mM
151	KCl, 148 mM NaCl, 1.3 mM CaCl ₂ , 0.9 mM MgCl ₂ , 0.7 mM NaH ₂ PO ₄ , 5.6 mM D-glucose and
152	10 mM HEPES, (~300 mOsm; pH 7.4; NaOH). 40 mM K ⁺ external solution was composed of 40

153 mM KCl, 104 mM NaCl, 1.3mM CaCl₂, 0.9mM MgCl₂, 0.7 mM NaH₂PO₄, 5.6 mM D-glucose



176 using the polygon selection tool with care to prevent overlapping regions. One region was

177 selected as the background; the values from this region were subtracted from each of the other 178 regions (ΔF). The equivalent of 30 seconds from the control condition of the time series were 179 used as the baseline fluorescence of all regions (F_{baseline}). The resulting equation is thus:

180 $\Delta F/F = (F_{\text{rol}} - F_{\text{background}})/F_{\text{baseline}}$

The data was then plotted as $\Delta F/F$ for every ROI in each frame. All results are represented as fold-change of $\Delta F/F$ with 1 representing baseline and 2 representing a doubling of calcium fluorescence. An ROI was considered responsive if its max $\Delta F/F$ was more than 3 standard deviations above the baseline before laser ablation and/or at the end of the recording. Neuronal area was calculated by dividing the total area of the ROIs containing a responsive neuronal segment divided by the total area of all neuronal ROIs visible in frame.

187To compare between videos and genotypes, traces were scaled with the maximum set at 1188 $(\Delta F/F = 1)$. This allowed for calculations of time of response within responsive ROIs. Total time189of response includes the time of the laser ablation to the time at which the trace has fallen to190within 3 standard deviations of the baseline fluorescence for at least five consecutive frames.191Time constants of decay (tau) were estimated by fitting to exponential decays using the Excel192add-in Solver.

NGAF Magnitude Analysis Videos were analyzed in ImageJ. All pixels above a
brightness level of 30 on a 0-255 scale were counted for each frame of the video (raw trace,
Figure 5). A sliding average of the previous 30 seconds was subtracted to generate the plots in
Figures 5D, 5H and Figure 9C. The area under the curve measurements were derived using the
Trapz function of Matlab. The area under the curve of all positive deflections (arbitrary units,
a.u.) describes the magnitude of the NGAF response.

199	Immunofluorescence Whole-mount immunostaining and imaging was performed as
200	previously described (Vyas et al., 2019). Briefly, grossly dissected inner ears were perfused with
201	4% PFA (Electron Microscopy Sciences, Inc., Hatfield, PA) in 1x PBS (Quality Biological Inc.,
202	Gaithersburg, MD) through the round window, then post-fixed for 30 minutes on a 3D-Rotator.
203	Mature inner ears were washed (3x30min) in PBS, then decalcified in 125 mM EDTA (Quality
204	Biological Inc., Gaithersburg, MD) in PBS for 2 hours before dissection into turns of the organ
205	of Corti. P7-10 inner ears were not decalcified before washing in PBS (3x30min) and dissection
206	into turns of the organ of Corti. Cochlear turns were immunolabeled with Goat anti-GFP (Sicgen,
207	Coimbra, Portugal, Cat# A32814, RRID:AB_2333099) to label GCaMP6f protein. Donkey anti-
208	Goat Alexa-488 (Invitrogen, Carlsbad, CA, Cat# AB0020-200, RRID:AB_2762838) was used
209	along with Alexa-647-conjugated Phalloidin (Thermofisher Scientific, Waltham, MA,
210	Cat#A22287, RRID:AB_2620155) and 4'6-Diamidine-2'-phenylindole dihydrochloride (DAPI,
211	Roche Molecular Systems, Inc., Branchburg,NJ) for GCaMP6f, hair cells, and nuclei,
212	respectively (Figure 1). Cochlear turns were mounted using ProLong Fade Gold Antifade
213	Mountant (Thermofisher Scientific, Waltham, MA, Cat# P36930) and imaged on a 700 LSM
214	Zeiss confocal microscope.
215	Immunofluorescence for Tac1 ^{Cre} ;Ai9 animals Immunofluorescence was performed as
216	described in the main methods sections with the following differences. Dorsal root ganglia were
217	dissected from mice as previously described (Sleigh et al., 2016). Dorsal root ganglia were not
218	decalcified. Cochleas and dorsal root ganglia from Tac1 ^{Cre} ; Ai9 animals were immunolabeled
219	with the following polyclonal antibodies: Goat anti-tdTomato (Sicgen, Coimbra, Portugal, Cat#

- AB8181-200, RRID:AB_2722750) and Rabbit anti-CGRP-α (Immunostar, Inc., Hudson, WI,
- 221 Cat# 24112, RRID:AB_572217). Alexa-568-conjugated Donkey anti-Goat (Invitrogen, Carlsbad,

222	CA, Cat# A-11057, RRID:AB_142581) and Alexa-488-conjugated Donkey anti-Rabbit
223	(Invitrogen, Carlsbad, CA, Cat# A-21206, RRID:AB_141708) secondary antibodies were used
224	for tdTomato and CGRP-a, respectively. Tac1 ^{Cre} ; Ai9 quantification of SGN neurons was based
225	on the previously published procedure for counting SGNs (Wu et al., 2018). Briefly, the organ of
226	Corti was divided into bins of 10% of the total length beginning at the apex (0%) to the base
227	(100%) and straight tangential lines segmented the SGN. SGNs within each bin were counted.
228	Auditory Brainstem Response (ABR) The ABR system, procedures and quantification
229	software used for this study have been previously described (Lauer and May, 2011; Lina and
230	Lauer, 2013). Mice were anesthetized with an intraperitoneal injection of 0.1cc per 20g body
231	weight of a mixture of ketamine (100 mg/kg) and xylazine (20 mg/kg) in 14% ethanol before
232	being placed on a gauze covered heating pad in the ABR chamber. The animals' eyes were
233	swabbed with petrolatum-based ophthalmic ointment to prevent corneal ulcers during anesthesia.
234	Subdermal platinum electrodes were placed at the vertex of the head (non-inverting), the left
235	pinna (inverting), and on the left side at the base of the tail (ground). 300 repetitions of a click or
236	pure-tone stimulus (10 stimuli/sec) were used to generate averaged ABR waveforms. Each tonal
237	stimulus was 5 ms in duration with a 0.5-ms rise and fall time. A Fostex dome tweeter speaker
238	(model FT28D) in a foam-lined chamber was used to present the stimuli to mice 30 cm away.
239	The ABR threshold was defined with custom MatLab software by calculating the averaged peak-
240	to-peak voltage during a 5-ms interval, beginning 1 ms after the onset of the stimulus, compared
241	to the averaged peak-to-peak voltage in a 5-ms window 20 ms after the stimulus. The threshold
242	was determined as the stimulus level where the peak-to-peak response was greater than 2
243	standard deviations above the electrical noise.

244	<i>Noise Exposure(s)</i> Mice were transferred to a low-noise, satellite housing facility from
245	the day before noise exposure through the endpoint for calcium imaging experiments. Due to the
246	susceptibility of the background strain, C57BL/6J, to age-related hearing loss, (Johnson, et al.,
247	1997) all experiments were performed with 6-week-old mice. Awake, unrestrained mice were
248	exposed to 110 dB SPL white noise for 2 hours in a set of interconnected cages fabricated from
249	wire mesh. Two set-ups were used to perform noise exposure. The first sound chamber and noise
250	exposure set-up has been previously described (NE-1) (Wu, et al., 2020). All other animals were
251	exposed to noise in a sound attenuating chamber with a reverberant lining (NE-2) (58cm x 40cm
252	x 30 cm; width, depth, height). NE-2 was equipped with 3 overhead, dome tweeter speakers
253	(Promaster TW47 1200W). Speakers were approximately 25 centimeters above the heads of the
254	mice. Broadband noise was generated by 2 JKT tone and noise generators (KV2 audio,
255	Milevsko, Czech Republic) powered by Neewer nw-100 phantom power sources (Shenzhen
256	Neewer Technology, Co. Guangdong, China). The noise generators were connected to 2 Crown
257	Drivecore XLS2502 amplifiers (Harman, Hemel Hempstead, UK): one driving a central speaker
258	in bridge mode and the other driving the two peripheral speakers in input Y mode. The decibel
259	level was tested in each set-up using a Larson-Davis LXT sound level meter (PCB Piezotronics,
260	Inc., Depew, NY) with a 1/2-in free field microphone. Care was taken to measure the sound level
261	at the position of the head of the experimental animals. The spectrum of the noise stimulus was
262	broadband with the highest energy from 2-20 kHz as measured by the Larson-Davis LXT sound
263	level meter.
264	Experimental Design and Statistical Analysis Power analysis was not performed to

265 determine sample size. Instead, experimental groups were designed to have >7 mice per group as

has been used for similar experiments (Weisz et al., 2009; Liu et al., 2015). Proportionate

267	numbers of both sexes were used throughout all experiments. Data was processed and analyzed
268	in R studio, Graphpad Prism, and Excel. The proportion of videos where at least one neuronal
269	ROI responds to focal ablation (neuronal response rate) is defined by the number of videos with
270	at least one responsive neuronal ROI divided by the total number of videos with at least one
271	visible, neuronal ROI responsive to 40 mM K^+ external solution. The proportion of videos with
272	visible NGAF over all videos is defined as the NGAF response rate. Statistical testing for
273	neuronal and NGAF response rate data used a generalized linear model with the family set to
274	binomial. Paired data within the same animal used the Wilcoxon ranked sum test. Data for ABR
275	results and spiral ganglion neuron counting were analyzed with ANOVA and used Dunnet's
276	comparison post-hoc test for multiple comparisons for the data in Figure 6E. Data that stemmed
277	from uneven numbers of multiple recordings across mice were analyzed with a linear mixed
278	model with the mouse identity as the random effect. Fixed effects are listed before each p-value
279	in the results section. For fixed effects or other tests with more than 2 levels a Bonferroni
280	correction was used to account for multiple comparisons. In figures, asterisks are used to
281	represent p-values as follows: * = p<0.05, ** = p<0.01, *** = p<0.001, **** = p<0.0001.
282	Correlation statistics were calculated with a linear regression. Original data and R files for
283	statistical testing are available upon request.
284	
285	RESULTS

286 Type-II-afferent-associated genes drive GCaMP6f expression

Type II afferents express several genes that differentiate them from type I afferents. Thus,
floxed fluorescent reporters driven by Cre-recombinase under the promoters of these genes
permit selective targeting of type II afferents. Two distinctive genes include tyrosine hydroxylase

290	(Th), which encodes the rate-limiting enzyme for the production of dopamine, and $Drd2$, which
291	encodes a dopamine receptor subunit (Molinoff and Axelrod, 1971; Daubner et al., 2011;
292	Kebabian and Calne, 1979). Th ^{2A-CreER} ;GCaMP6f provided an apically-biased gradient of type II
293	cochlear afferent expression and <i>Drd2^{Cre};</i> GCaMP6f targeted basally-biased type II cochlear
294	afferents as schematized in Figure 1H. Expression of GCaMP6f was confirmed first with
295	immunohistochemistry and recapitulated the reported expression patterns for each genotype
296	(Figure 1B, E) (Vyas, et al., 2017; Wu et al., 2018; Vyas et al., 2019). Cre-driven expression of
297	floxed GCaMP6f was especially apparent in the peripheral dendrites of type II afferents
298	underneath the rows of OHCs for both genotypes (Figure 1C, F) even more so than Tuj1
299	immunostaining, a general neuronal marker (Figure 1c1-3). Medial olivocochlear neurons as
300	confirmed by Tuj1 staining showed no appreciable expression of GCaMP6f; but, there was some
301	expression in lateral olivocochlear neurons (LOCs) in Th ^{2A-CreER} ;GCaMP6f and
302	Drd2 ^{Cre} ;GCaMP6f animals as described previously for tdTomato expression (Figure 1C; Wu et
303	al., 2020; Vyas et al., 2019). However, LOC neurites are restricted to the IHC region and thus
304	never interfered with imaging type II afferents under the OHCs.
305	Two-photon microscopy was used to image type II afferents in an otic capsule
306	preparation (Sirko et al., 2019) (Figure 1A, D, G). This allowed for imaging of type II afferents
307	throughout the cochlear spiral. For animals over 4 weeks of age, the spiral otic capsule was
308	excised from the temporal bone. The apical cochlear turn was revealed by removing the bony tip
309	of the cochlea (Figure 1A). Further dissection revealed more basal regions (Figure 1D). This
310	method preserved the architecture of the older cochlear tissue in contrast to complete soft tissue
311	excision as used in previous studies. Additionally, the otic capsule preparation reduced the
312	amount of damage to the tissue, especially in older cochleas when the bone has ossified. In pre-

hearing animals, both the acutely excised preparation and otic capsule preparation were used, but the otic capsule preparation was preferred to mirror the conditions of the mature preparations. While the otic capsule preparation is quicker and causes less tissue disruption, the tissue is uneven and much thicker, requiring multiphoton microscopy to overcome the curvature and opacity of the tissue.

318 Description of Calcium Imaging Protocol

319 GCaMP6f signals were recorded from type II afferents in pre-hearing tissue following focal 320 ablation of nearby OHCs. Experiments followed a stereotyped protocol illustrated in Figure 2. 321 First, type II afferent dendrites were visualized underneath the rows of OHCs in the presence of 322 15 or 40 mM K⁺ solution where fluorescence in the dendrites was consistently bright. Once dendrites were located, 5.8 or 2.5 mM K⁺ solution replaced the bath solution to recover possible 323 324 desensitization from the high potassium solution and establish a baseline fluorescence level. 325 Type II afferent activity was recorded for 30 seconds at the start of each video to establish the 326 baseline for normalization of calcium responses (Figure 2a1-2). OHCs were ruptured through 327 photoablations caused by iterations of 100% power from a 2-photon laser focused on a hand-328 drawn region of interest the size of 1-3 OHCs (Gale et al., 2004; Sirko et al., 2019). Imaging 329 could not occur during laser ablation, therefore a gap occurs in imaging in each trial for a median 330 time of 8.4 seconds represented by a red bar in the timeline (Figure 2A) and above recordings 331 (Figure 2b4). After this time, imaging typically lasted for about 4.5 minutes after the end of laser 332 ablation to capture the full response of the type II afferents (Figure 2a3-6, 2b4). Dendrites were 333 visualized by generating projection images where each pixel was scaled in gray according to its 334 change in brightness relative to the standard deviation of the baseline fluorescence over either 335 part of or for the entire recording ("standard deviation image", Figure 2a2, 2a4, 2a6, 2b1-3).

336	Once type II dendrites were located in standard deviation images, hand-drawn regions of interest
337	(ROIs) were drawn in ImageJ around each visible portion of the neuron, making sure to avoid
338	overlap between multiple dendrites (Figure 2b2). The fluorescence levels for each neuronal ROI
339	were measured for each frame. Then the fluorescence of a background ROI was subtracted from
340	the neuronal fluorescence for each frame. The difference of these values was then divided by the
341	average fluorescence of the neuronal ROI in the 30 second baseline period ($\Delta F/F$). The $\Delta F/F$
342	values for each ROI signify the fold change in brightness over the baseline with 1 representing
343	baseline brightness and a value of 2 as a doubling in the brightness. Each individual ROI was
344	classified as responsive if its $\Delta F/F$ trace rose above three standard deviations from the baseline
345	brightness and decreased by at least three standard deviations before reaching the eventual steady
346	state value (Figure 2b4). Individual ROIs that met this criterion are shown as yellow outlined
347	ROIs in each figure. The white arrow in Figure 2b2-3 indicates the trace for an example
348	responding region of interest.
349	Tissue damage can evoke calcium responses in apical and basal type II cochlear afferents

350 Following ablations that caused visible tissue damage, at least one type II neurite within the field 351 of view experienced a transient increase in fluorescence in pre-hearing tissue 58% (26/45) of the 352 time (neural response rate is defined as #Photoablation with neural response / (#Photoablation 353 with neural response + #Photoablation without neural response), Table 2). Figure 3 shows the response of pre-hearing, apical and basal type II afferents following photoablation using Th^{2A-} 354 CreER; GCaMP6f and Drd2^{Cre}; GCaMP6f mice, respectively. An example of a photoablation in the 355 apex of a pre-hearing, Th^{2A-CreER};GCaMP6f animal is shown in Figure 3A. Figure 3B highlights 356 357 the regions of interest used in analysis of type II afferent segments where each yellow, outlined 358 region responded to the photoablation. The responses to damage in pre-hearing, type II afferents

359	from <i>Th</i> ^{2A-CreER} ;GCaMP6f or <i>Drd</i> 2 ^{Cre} ;GCaMP6f mice typically decreased monotonically from
360	the first image after laser ablation (Figure 3C,D,F,G). The overall time from when the $\Delta F/F$ first
361	rose above three standard deviations of the baseline to within three standard deviations of the
362	steady state value was defined as the response duration and is represented by the black bar above
363	Δ F/F plots. The average response duration for pre-hearing type II afferents was 45.5s ± 25.0s
364	(Figure 3C, 3D). Considering the median gap time of 7.2 seconds in imaging during and after
365	photoablation, these response times are similar in length to the membrane currents (90% decay
366	time of 58.5s) measured by tight-seal intracellular recordings from type II afferents (Liu et al.,
367	2015). This suggests that the GCaMP6f fluorescence closely follows the electrical response of
368	the type II afferent to acute damage.
369	Transient calcium events occurred in type II afferents of the apex (Th ^{2A-CreER} ;GCaMP6f
370	animals, Figure 3A-D) and base (<i>Drd2^{Cre}</i> ;GCaMP6f animals, Figure 3E-G) of the cochlea.
371	Although these particular examples have markedly different time courses, overall there were no
372	significant differences in response probability or time course as a function of cochlear position.
373	For all videos recorded from pre-hearing animals, the proportion of videos with at least one,
374	visible, responding neuron was similar for both classes of neurons (neural response rate; Table 2;
375	Th 11/35 videos vs. Drd2 24/53 videos; $p = 0.099$, generalized mixed model) as were the
376	response durations (Figure 4E; <i>Th</i> : 54.6 ± 9.7 s vs. <i>Drd2</i> : 43.2 ± 32.5 s; p = 0.34, linear mixed
377	model Satterthwaite's method). Therefore, all following reported averages will reflect pooled Th
378	and Drd2 data, even though the effect of genotype was always factored into statistical analyses.
379	ATP contributes to the damage response of pre-hearing type II afferents
380	ATP is a major contributor to the response of type II cochlear afferents to focal OHC ablation

381 (Liu et al., 2015). Blocking purinergic receptors with 100 µM pyridoxalphosphate-6-azophenyl-

382	2',4'-disulfonic acid (PPADS), a generic P2X and partial P2Y receptor antagonist, greatly
383	reduced the duration, but not the peak amplitude of a damage-evoked inward current in apical
384	pre-hearing type II cochlear afferents (Liu et al., 2015). Using calcium imaging, bath applied 100
385	μM PPADS did not prevent neuronal responses to photoablation (Figure 4A-C) and had no
386	significant effect on the probability of a type II GCaMP6f response to damage within the field of
387	view (neural response rate, Table 2; PPADS 8/12 videos vs control 20/31 videos). This is
388	consistent with the ability of 100 μ M PPADS to abbreviate but not completely block the
389	damage-evoked membrane current in type II cochlear afferents (Liu et al., 2015). Also, 100 μ M
390	PPADS did not significantly alter the duration of the calcium signal in pre-hearing type II
391	afferents (Figure 4D; no PPADS: $40.4s \pm 25.5s$ vs. PPADS $48.2s \pm 31.5s$, n = 14 videos, N = 8
392	mice). However, 100 μ M PPADS did significantly restrict the extent of activation of type II
393	afferents within the field of view. This was measured as the summed area of responding type II
394	ROIs as a fraction of the area of all type II ROIs in the field of view, hereafter referred to as
395	neural response area (Figure 4E: Control: 62.7% \pm 26.0% vs. PPADS: 37.7% \pm 21.8%, p =
396	0.00011, df = 5.34, n = 15 videos, N = 9 mice, linear mixed model Satterthwaite's method). This
397	observation supports the hypothesis that ATP release among surrounding supporting cells
398	promotes the spatial and temporal spread of the response to damage (Gale et al., 2004; Liu et al.,
399	2015; Sirko et al., 2019).
400	Non-GCaMP6f-associated fluorescence reflects epithelial cell activity and depends on ATP
401	Previous studies used membrane permeant dyes to describe ATP-dependent calcium waves
402	propagating through cochlear supporting cells after acute tissue damage (Anselmi et al., 2008;
403	Gale et al., 2004; Sirko et al., 2019). In the present work, temporal and spatial variations in
404	fluorescence were evident even in tissue that did not express the indicator GCaMP6f; referred to

405	henceforth as Non-GCaMP6f-Associated-Fluorescence or NGAF events, presumably resulting
406	from tissue-dependent changes in the optical path. NGAF events appeared transiently in large
407	swaths of tissue either in the greater epithelial ridge region (Figure 5A-C) or in the area of the
408	OHCs (Figure 5E-G) in pre-hearing animals. Given their location and duration, NGAF events are
409	likely to be the consequence of ATP-dependent waves among supporting cells. This activity was
410	observed originally by differential interference contrast (DIC) imaging due to the physical
411	shrinkage and increased extracellular space from ionic flux and associated water loss, termed
412	crenation (Babola et al., 2020; Tritsch et al., 2007; Tritsch et al., 2010). The sensitivity of the 2-
413	photon microscope used in the present experiments enables detection of crenations among
414	supporting cell tissue as the transmitted fluorescence varies with optical density.
415	NGAF activity occurred spontaneously (Figure 5A-C) or immediately following focal
416	OHC ablation (Figure 5E-G). Both spontaneous and evoked NGAF events occurred in a mouse
417	with no GCaMP6f expression in any cell type under similar recording conditions (Figure 5A-D,
418	Video 3). Negative immunostaining for GCaMP6f additionally confirmed that NGAF is not due
419	to ectopic expression of GCaMP6f in non-neuronal cells of the organ of Corti.
420	The magnitude of NGAF activity was calculated as the area under the curve of
421	deflections in brightness over an arbitrary threshold (Figure 5D,H). The presence of 100 μ M
422	PPADS caused no significant effect on NGAF magnitude when pooling across animals as
423	measured by the area under the curve of NGAF activity (data not shown). This may be due to the
424	large variability observed across animals. To circumvent the differences between animals, paired
425	recordings were compared in the same cochlea for focal ablations at different locations. Shifting
426	the location of focal ablation did not have a significant effect on the NGAF magnitude as the
427	magnitude was just as likely to increase as decrease when ablation was repeated in control

428	solutions (Figure 5I, $p = 0.66$, $N = 28$ cochleas, Paired Wilcoxon Signed Rank Test). In contrast,
429	paired videos where the second ablation occurred with 100 μ M PPADS in the bath had a reduced
430	NGAF magnitude compared to preceding activity 15 out of 19 times (Figure 5J; $p = 0.0071$, $N =$
431	19 cochleas, Paired Wilcoxon Signed Rank Test). Overall, the dynamics, location, and ATP-
432	dependence of NGAF activity support the interpretation that these are another sign of the
433	previously reported activity waves among cochlear supporting cells (Gale et al., 2004; Ceriani et
434	al., 2019; Sirko et al., 2019).
435	Generation and verification of the Tac1 ^{Cre} ;GCaMP6f mouse model
436	Although NGAF activity corresponds to supporting cell activity, it is not as bright or distinct as
437	the fluorescence emitted from GCaMP6f expressing cells. A better system would exploit
438	GCaMP6f fluorescence in both supporting cells and type II cochlear afferents. This proved
439	possible using a peculiarity in expression of the Tac1 gene by cochlear tissue. Alternative
440	splicing of the Tac1 gene leads to the production of four different neuropeptides, including
441	substance P (Krause et al., 1987). Tac1 is expressed by peptidergic somatosensory neurons in the
442	dorsal root ganglia (Figure 6F) (Weissner et al., 2006; Kestell et al., 2015). RNA-seq from
443	cochlear afferents suggested that type II cochlear afferents and one subtype of type I cochlear
444	afferents could express Tac1 (Shrestha et al., 2018). Tac1 ^{Cre} mice crossed with Ai9 (floxed
445	tdTomato) reporter mice exhibited a unique expression pattern: whereby nearly every hair cell
446	and supporting cell in the cochlear apex expressed tdTomato (Figure 6A), but with a progressive
447	absence of expression in epithelial cells towards the cochlear base (Figure 6B). In sharp contrast,
448	a subset of SGNs expressed tdTomato throughout the cochlear length except at the extreme
449	apical tip where SGNs are few (Vyas et al., 2019) (Figure 6E; df = 9, f value = 3.104, p =
450	0.0082, N = 5 animals, one-way ANOVA). Excluding the first 10% of the cochlea, there were no

451	significant differences in SGN expression of tdTomato among the remaining areas along the
452	cochlear spiral (df = 8, f value = 1.605, $p = 0.17$, $N = 5$ animals, one-way ANOVA). The total
453	number of SGNs expressing tdTomato was equivalent to all type II cochlear afferents plus a
454	minority of type I cochlear afferents. Type II afferent identity was confirmed by taking higher
455	magnification confocal images of Tac1 ^{Cre} ; Ai9 cochleas in the OHC region. Many of the
456	fluorescent fibers turned basally, ran parallel underneath the OHCs (Figure 6C,D) and projected
457	bouton endings to OHCs (Figure 6d1,3), confirming their type II afferent identity.
458	Type II afferent and epithelial cell calcium activity in Tac1 ^{Cre} ;GCaMP6f mice
459	Tac1 ^{Cre} mice were crossed with floxed GCaMP6f mice to express GCaMP6f in all cell types that
460	have expressed Tac1 at any point in development. In the apex of the cochlea, calcium imaging in
461	pre-hearing mice recapitulates observations of spontaneous crenations and widespread calcium
462	responses to damage (data not shown) (Gale et al., 2004; Tritsch et al., 2007). The most
463	informative Tac1 expression pattern, however, is in the middle turn of the cochlea where there is
464	stochastic expression in epithelial cells, providing concurrent viewing of type II cochlear afferent
465	neurites through the gaps in epithelial cell expression (Figure 7A). Analysis of videos in this
466	region of the cochlea facilitates the simultaneous observation of calcium events in epithelial cells
467	(Figure 7B) and type II cochlear afferents (Figure 7C). Pre-hearing type II afferents labeled by
468	<i>Tac1^{Cre}</i> are capable of responding to local photoablation (neural response rate, Table 3; 22/36
469	videos). The average response duration for epithelial cells and neurons statistically indistinct
470	(Figure 7H).
471	When examining the base of the cochlea, the GCaMP6f expression is mostly restricted to

472 neurons (Figure 7D). Thus, NGAF response duration is used as a measure of epithelial response 473 to photoablation. The response duration of neurons, NGAF, and epithelial cells are statistically

474	insignificant (Figure 7H.) Individual epithelial cells may have a staggered, short (Figure 7E) or
475	repeating (Figure 7G) response to photoablation. However, when averaged, the total time of
476	response for all epithelial cells is not distinguishable from the response durations of neurons or
477	NGAF (Figure 7H; NGAF: 59.9 \pm 35.6 s, type II GCaMP6f: 50.1 \pm 37.3 s, vs epithelial cell
478	GCaMP6f: 54.2 ± 29.2 s, $p_{epithelial cell} = 0.91$ df = 24.2, $p_{NGAF} = 1.0$ df = 22.9, $p_{type II} = 1.0$ df =
479	19.2; $n = 20$ videos, $N = 14$ cochleas, linear mixed model Satterthwaite's method with
480	Bonferroni correction). This suggests that NGAF activity is not an exact readout of calcium
481	signaling within individual epithelial cells; but, instead, demonstrates the summed activity of
482	epithelial tissue.
483	Type II cochlear afferent responses to tissue ablation are less frequent and longer-lasting in
484	mature cochleas
485	Calcium imaging of otic capsule preparations enabled study of fully mature tissue for which
486	intracellular recording is difficult. Mature (between 6-10 weeks of age) type II cochlear afferents
487	were capable of responding to focal OHC ablation; however, responses occurred about one third
488	as often as in cochleas from pre-hearing animals. This reduced response probability to damage

s as often as in cochleas from pre-hearing animals. This reduced response probability to damage 488 489 was based only on those cases where OHC damage and type II afferent dendrites were clearly 490 visible (neural response rate, Table 2; mature: 9/43 vs pre-hearing: 26/47, p = 0.00046, N = 22 491 cochleas, generalized mixed model). In mature cochleas damage occurred less reliably. The 492 decrease in response rate to damage could not be explained by a decrease in the amount of 493 damage caused by the focal laser ablations. When it occurred, the area of damage was not 494 significantly different in size between the pre-hearing and mature animals. Rather, independent 495 of age, scar caused by the laser was significantly larger in cases where the damage caused type II afferent responses (with response: $305.8 \pm 251.6 \ \mu\text{m}^2$ vs. without response: $209.8 \pm 182.7 \ \mu\text{m}^2$, p 496

497	= 0.009, df = 118.4, n = 153 videos, N = 72 cochleas, linear mixed model, Satterthwaite's
498	method). This points to a correlation between the amount of damage and the neuronal response,
499	or perhaps a threshold for evoking neuronal responses.
500	Type II afferents from mature $Th^{2A-CreER}$, and $Drd2^{Cre}$ (Figure 8A-C), as well as $Tac1^{Cre}$
501	(Figure 8D-F) animals expressing GCaMP6f responded to focal ablation of OHCs. As before,
502	ROIs with colored outlines in each standard deviation plot represent the location of type II
503	afferent dendrites or epithelial cells that respond to the focal ablation (Figure 8A,D). The Δ F/F
504	traces of each responsive element in each example are shown in Figure 8B and E and the
505	averages for each recording in Figure 8C and F. The time of response was significantly longer in
506	mature compared to pre-hearing animals (Figure 8G; mature: 73.5 \pm 53.8s vs pre-hearing: 42.5 \pm
507	25.0s, $p = 0.020$, $df = 18$, $n = 42$ videos, $N = 27$ cochleas, linear mixed model Satterthwaite's
508	method). The neuronal response area was significantly reduced in mature compared to pre-
509	hearing responses (Figure 8H; pre-hearing: $63\% \pm 26\%$ vs. mature: $41\% \pm 15\%$, p = 0.0030, df =
510	23.5, $n = 35$ videos, $N = 14$ cochleas, linear mixed model Satterthwaite's method). Furthermore,
511	the frequency of NGAF activity was reduced in mature tissue compared to pre-hearing tissue
512	(NGAF response rate defined as # with NGAF/ (# with NGAF + # without NGAF), Table 2;
513	mature: $51/144$ vs. pre-hearing: $73/117$, p = 2.18×10^{-6} , N = 52 cochleas, generalized mixed
514	model). Also, the NGAF magnitude in mature tissue decreased relative to that found in pre-
515	hearing tissue (Figure 8I; pre-hearing: 13.4 ± 56.9 a.u. vs. mature: 3.3 ± 8.4 a.u., p = 0.0346, df =
516	31.2, $n = 73$ videos, $N = 35$ cochleas, linear mixed model Satterthwaite's method). When NGAF
517	activity did occur in mature tissue, it was situated mostly in the OHC region instead of the
518	greater epithelial ridge as was the case in the pre-hearing animals (Figure 5E) (Sirko et al.,

519	2019). Overall, while mature cochlear tissue still could respond to focal damage, such responses
520	were less frequent, less extensive, but longer-lasting than those in the pre-hearing cochlea.
521	Acoustic trauma enhances type II afferent and epithelial responses to focal ablation
522	The present methods apply to type II afferents in older cochlear tissue, enabling the study of the
523	effects of previous acoustic trauma on the acute damage responses. Mice were exposed to 2
524	hours of 110 dB broadband noise, then compared to their control, untraumatized littermates 7 or
525	21 days later. No difference was observed between mice 7 or 21 days after noise exposure;
526	therefore, data from these mice have been grouped together. Noise-exposed mice had a
527	significant increase in ABR thresholds measured the day before calcium imaging experiments as
528	compared to littermate controls and wild-type mice (Figure 9A; two-way ANOVA, Drd2: p =
529	<0.0001, F (2 DFn, 42 DFd) = 49.59; <i>Th</i> : p = <0.0001, F (2 DFn, 102 DFd) = 38.45). A unique
530	feature of responding neuronal ROIs after noise exposure was a brief calcium transient to
531	photoablation followed by a secondary, delayed response several minutes after the initial change
532	in GCaMP6f fluorescence. Δ F/F traces of type II afferent dendrites in this example from a <i>Th</i> ^{2A-}
533	CreER;GCaMP6f mouse reveal an initial response to the focal ablation followed by increases over
534	the next few minutes (Figure 9B). As in the previous pre-hearing and mature cochleas, NGAF
535	activity was observed alongside neuronal responses and occasionally mirrored the delayed
536	pattern seen in the neurons. All together, over the various genotypes, ages, and noise exposure
537	statuses there was a significant correlation between the proportion of times we observed NGAF
538	activity and neuronal responses to damage in all videos of each condition (Figure 9C; $R^2 = 0.78$,
539	p-value = 0.020 F (1 DFn, 4 DFd) = 13.98). Figure 9D and E show an example of the extent of
540	both the neuronal and epithelial cell responses immediately following focal ablation (D) and at
541	the end of the recording (E). Increases in epithelial cell fluorescence are visualized by measuring

542	the increases in the percentage of pixels above an arbitrary brightness (Figure 9F) and reveal the
543	repetitive nature of the delayed NGAF responses. A late secondary neuronal response was
544	significantly more likely in mice that were noise exposed over all other mature animals (Figure
545	9G; noise-exposed: 7/31 vs. non-noise-exposed: 4/77, p = 0.036, N = 23 animals, Fisher's exact
546	test for count data with Bonferroni correction for multiple comparisons), although delayed
547	responses were present in some non-noise exposed mice (see arrow in Figure 8C for an
548	example). The observation that both NGAF and neuronal responses display secondary responses
549	after noise exposure strengthens the correlation between NGAF and neuronal responses.
550	However, it is unclear at this time if these are causally related, or independent responses to the
551	initial damage.
552	
553	
554	DISCUSSION
555	
556	GCaMP6f expression in type II afferents reveals a calcium response to focal ablation in mature
557	and noise exposed mice
558	Calcium imaging using Cre-driven GCaMP6f expression expands functional studies of type II
559	afferents in the cochlea. This method coupled with 2-photon microscopy of an otic capsule
560	preparation enables recording of type II activity throughout the entire cochlea of mature mice.
561	Calcium signals in type II afferent dendrites extend and add to the previous description of
562	electrical signals evoked by ATP and OHC rupture in pre-hearing animals (Weisz et al., 2009;
563	Weisz et al., 2012; Weisz et al., 2014; Liu et al., 2015). The fluorescent response to calcium

immediately after focal laser ablation is similar in time course to the depolarization observed in

pre-hearing type II afferents after OHC rupture (Liu et al., 2015). But in addition, these studies of the mature, and post-trauma cochlear tissue have revealed activity patterns not seen in younger cochleas. Development of more Cre mouse lines to target subtypes of type I or type II afferents specifically provides an opportunity to expand the use of this technique for cochlear neuroscience.

570 Focal ablation produced similar responses in type II afferents distinguished by gene 571 expression and location along the cochlear tonotopic axis. The genes that define the two mouse 572 models used in the majority of this study, Th and Drd2, are part of the dopamine production and 573 response pathway and target apical and basal type II afferents respectively (Daubner et al., 2011; 574 Beaulieu and Gainetdinov, 2011; Vyas et al., 2017; Wu et al., 2018; Vyas et al., 2019). The 575 genes encoding CGRP- α and SERT also mark specific populations of type II afferents along the 576 tonotopic axis (Vyas et al., 2019). Targeting these various neurotransmitter and neuropeptide 577 pathways may help tease apart functional differences between these genetically distinct type II 578 afferents.

579 Maturation and the onset of hearing had significant effects on type II afferent responses 580 to damage. Mature type II afferents can respond to focal damage of the organ of Corti, albeit 581 with lower probability and longer time course, when compared to pre-hearing neurons. The 582 reduction in neuronal response probability correlated with a reduction in the frequency of 583 supporting cell activity (here called NGAF activity) in mature tissue, implying that epithelial cell 584 activity is related to type II afferent responses, presumably through the release of ATP or other 585 activators (Cook and McCleskey, 2002; Gale et al., 2004; Tritsch et al., 2007; Talagas et al., 586 2020).

589 *hearing cochleas*

590 ATP is important for refining neuronal circuitry and activity in pre-hearing animals for multiple 591 cochlear cell types including type II afferents (Ceriani et al., 2019; Tritsch et al., 2007; Tritsch et 592 al., 2010). Beyond spontaneous events, ATP release in the cochlea can be elicited by cell rupture 593 and then propagated through ATP mediated ATP release in the cochlear epithelium (Gale et al., 594 2004; Cook and McCleskey, 2002). This amplification after damage is evident in the widespread 595 NGAF and type II neuron responses. In pre-hearing animals, the proportion of type II afferents 596 that experienced calcium transients to acute photoablation was reduced in the presence of 597 PPADS, indicating that ATP release from epithelial cells increases the number of activated type 598 II afferent neurons. This corresponds with previous observations that ATP-evoked inward 599 currents of type II afferents were abbreviated similarly by PPADS or connexin block (Liu et al., 600 2015) as though produced by connexin-dependent release of ATP from supporting 601 cells. Unfortunately, direct observation of calcium waves spreading throughout the epithelium 602 was hindered by the seconds-long lag in recording following photoablation. Alternative 603 approaches that reduce the lag time could clarify how the calcium wave propagates after insult 604 and reveal faster calcium transients. 605 606 Non-GCaMP6f-associated Fluorescence is correlated with neuronal activity

607 In mature cochleas, the NGAF magnitude was smaller than in pre-hearing cochleas, and fewer 608 type II afferents responded after damage. The remaining NGAF activity is no longer spontaneous 609 and thus most likely represents the "slow waves" observed by Sirko et al., where ATP-

610 independent calcium responses spread among the supporting cells of the organ of Corti (Sirko et

611	al., 2019). Additional experiments are necessary to learn if there is a causal link between
612	epithelial cell activity and neuron activation especially in the mature cochlea. The location,
613	timing, and ATP-dependence of NGAF activity suggest that it represents epithelial cell activity;
614	however, these measurements were indirect. An ideal mouse model would combine the ability to
615	compare NGAF activity with direct measurements of epithelial cell calcium signals while
616	maintaining the ability to measure neuronal responses. Serendipitously, Tac1 ^{Cre} expression of
617	GCaMP6f varied along the cochlear length to provide that opportunity. In the mid-cochlea,
618	Tac1 ^{Cre} ;GCaMP6f labelled all type II neurons, but produced a mosaic of epithelial expression,
619	revealing the tight correlation between epithelial cell and type II afferent activity. Average
620	NGAF activity and GCaMP6f responses had a similarly extended time of response after focal
621	ablation, even though individual epithelial cell GCaMP6f signals were markedly shorter in
622	duration. The similarity of NGAF event and epithelial cell GCaMP6f activity supports the claim
623	that NGAF activity reflects the calcium responses of the epithelial cells. Thus, the larger changes
624	in NGAF activity with maturation reveal the shift from spontaneous, fast events to infrequent,
625	slow waves after the onset of hearing.
626	

627 Similarities between type II afferents and somatic nociceptors

Building on previous studies of gene expression, morphology and function, the expression of *Tac1* strengthens the hypothesis that type II afferents are cochlear nociceptors. Type II afferents
and somatosensory C-fibers both have a thin, unmyelinated, highly branched morphology. Cfibers in the somatosensory system report tissue damage (Cook and McCleskey, 2002); similarly,
pre-hearing type II afferent neurons respond to cell rupture (Liu et al., 2015). C-fibers and type II
afferents also share gene expression including *Tac1*, as well as *Calca* and *Th* (Wu et al., 2018; Le

634 Pichon and Chesler, 2014). Somatosensory nociceptors can become sensitized and release 635 CGRP-a and substance P after tissue damage (Li et al., 2008; Andrew and Greenspan, 1999; 636 Smith et al., 2013; Murthy et al., 2018). Previous studies have shown an effect of substance P 637 directly on SGNs and a protective effect of substance P after acoustic trauma (Nario et al., 1995; 638 Sun et al., 2004; Ito et al., 2002; Kanagawa et al., 2014). Therefore, additional study of the effect 639 of substance P on type II afferents in the context of acute damage is needed. 640 Calcium imaging offers an opportunity to study changes in mature type II activity 641 following acoustic trauma. Delayed responses occurring minutes after the initial tissue damage 642 in type II afferents and epithelial cells became more common after acoustic trauma. The timing

of the onset of delayed responses suggests that these could occur via G-protein coupled receptor pathways and/or post-translational modifications, although the specific mechanism is unknown (Hoare et al., 2020; Gold, 1999). Increased somatosensory pain can occur within the same time frame (2-5 min) as the delayed cochlear responses to acute tissue damage after acoustic trauma. Increased somatic pain also involves inflammation leading to NMDAR subunit phosphorylation downstream of PKC (Guo et al., 2002). It remains to be seen if inflammation plays a role in the prolonged response to acute damage in the cochlea.

Another possible mechanism of delayed responses can be seen in another somatosensory system. Spinal cord circuits involved in itch rely on burst action potential firing to induce neuropeptide release that drives sustained firing in downstream neurons by closing KCNQ channels (Pagani et al., 2019). KCNQ channels were implicated in the type II afferent response to damage (Liu et al., 2015) and type II afferents appear to express genes for KCNQ channels and several neuropeptides including CGRP and Substance P (Lallemend et al., 2003; Wu et al., 2018; Vyas et al., 2019; Shrestha et al., 2018) indicating that neuropeptide release in the noise-

657 damaged cochlea could explain the sustained calcium activity observed in type II afferent

658 dendrites following acoustic trauma.

659

660 Putative role of type II afferents in pathological hearing

661 Hearing loss subsequent to acoustic trauma is correlated with increased synaptic ribbons 662 in the OHCs, predicting a functionally significant increase in the number of type II afferent 663 action potentials (Wood et al., 2021). The prolonged depolarization of type II afferents indicated 664 by GCaMP6f imaging could further lower the threshold for activation by transmission from 665 OHCs during sound. If type II afferents are equivalent to nociceptors, their increased activation 666 after hearing loss, in combination with synaptopathic loss of type I afferent activity (Stamataki et 667 al., 2006; Kujawa and Liberman, 2009), could cause innocuous sound to become aversive. 668 However, it is still unclear if type II afferents contribute to pathological changes following 669 traumatic noise exposure. For example, painful hyperacusis is a common sequela of acoustic 670 trauma and is characterized by a decrease in the intensity at which sound becomes painful, 671 mirroring the greater sensitivity and longer duration responses to stimulation seen in somatic 672 pain syndromes such as allodynia and hyperalgesia (Pienkowski et al., 2014; Tyler et al., 2014; 673 Jensen and Finnerup, 2014). Modulation of type II activity therefore provides a possible 674 therapeutic target for damage-induced hyperacusis. Further study is required however to develop 675 a sufficiently robust animal model for hyperacusis to test the connection between hyperacusis 676 and altered type II afferent function. 677 678

680 REFERENCES

681	Andrew D, Greenspan JD (1999) Mechanical and heat sensitization of cutaneous
682	nociceptors after peripheral inflammation in the rat. J Neurophysiol 82:2649-265.
683	Anselmi F, Hernandez VH, Crispino G, Seydel A, Ortolano S, Roper SD, Kessaris N,
684	Richardson W, Rickheit G, Filippov MA, Monyer H, Mammano F (2008) ATP release through
685	connexin hemichannels and gap junction transfer of second messengers propagate Ca ²⁺ signals
686	across the inner ear. Proc Natl Acad Sci. 105:18770-18775.
687	Babola TA, Kersbergen CJ, Wang HC, Bergles DE (2020) Purinergic Signaling in
688	cochlear supporting cells reduces hair cell excitability by increasing the extracellular space.
689	eLife. 9:e52160.
690	Beaulieu JM, Gainetdinov RR (2011) The physiology, signaling, and pharmacology of
691	dopamine receptors. Pharmacol Rev. 63:182-217. Review.
692	Berglund AM, Ryugo DK (1987) Hair cell innervation by spiral ganglion neurons in the
693	mouse. J. Comp. Neurol. 1255:560-70.
694	Brown MC (1994) Antidromic responses of single units from the spiral ganglion. J.
695	Neurophysiol. I71:1835-1847.
696	Ceriani F, Hendry A, Jeng J-Y, Johnson SL, Stephani F, Olt J, Holley MC, Mammano F,
697	Engel J, Kros CJ, Simmons DD, Marcotti W (2019) Coordinated calcium signalling in cochlear
698	sensory and non-sensory cells refines afferent innervation of outer hair cells. The EMBO
699	Journal. 38:e99839.
700	Cook SP, McCleskey EW (2002) Cell damage excites nociceptors through release of
701	cytosolic ATP. Pain. 95:41-7.

702	Daubner SC, Le T, Wang S (2011) Tyrosine hydroxylase and regulation of dopamine
703	synthesis. Arch Biochem Biophys. 508:1-12. Review.
704	Flores EM, Duggan A, Madathany T, Hogan A, Márquez FG, Kumar G, Seal RP,
705	Edwards RH, Liberman MC, García-Añoveras J (2015) A non-canonical pathway from cochlea
706	to brain signals tissue-damaging noise. Curr. Biol. 25:606-12.
707	Gale JE, Piazza V, Ciubotaru CD, Mammano F (2004) A mechanism for sensing noise
708	damage in the inner ear. Curr. Biol. 14:526-9.
709	Ghimire SR, Deans MR (2019) Frizzled3 and Frizzled6 cooperate with Vangl2 to direct
710	cochlear innervation by type II spiral ganglion neurons. J Neurosci. 39:8013-8023.
711	Guo W, Zou S, Guan Y, Ikeda T, Tal M, Dubner R, Ren K (2002) Tyrosine
712	phosphorylation of the NR2B subunit of the NMDA receptor in the spinal cord during the
713	development and maintenance of inflammatory hyperalgesia. J Neurosci. 22:6208-17.
714	Hoare SRJ, Tewson PH, Quinn AM, Hughes TE, Bridge LJ (2020) Analysing kinetic
715	signaling data for G-protein-coupled receptors. Scientific Reports. 10:12263.
716	Ito K, Rome C, Bouleau Y, Dulon D (2002) Substance P mobilizes intracellular calcium
717	and activates a nonselective cation conductance in rat spiral ganglion neurons. Eur J Neurosci.
718	16:2095-102.
719	Jensen TS, Finnerup NB (2014) Allodynia and hyperalgesia in neuropathic pain: clinical
720	manifestations and mechanisms. Lancet Neurol. 13:924-35. Review.
721	Johnson KR, Tian C, Gagnon LH, Jiang H, Ding D, Salvi R (2017) Effects of Cdh23

- single nucleotide substitutions on age-related hearing loss in C57BL/6 and 129S1/Sv mice and
- 723 comparisons with congenic strains. Scientific Reports. 7:44450.

724	Johnson KR, Erway LC, Cook SA, Willott JF, Zheng QY (1997) A major gene affecting
725	age-related hearing loss in C57BL/6J mice. Hearing Research. 114:83-92.
726	Kanagawa E, Sugahara K, Hirose Y, Mikuriya T, Shimogori H, Yamashita H (2014)
727	Effects of substance P during the recovery of hearing function after noise-induced hearing loss.
728	Brain Research. 1582:187-96.
729	Kebabian JW, Calne DB (1979) Multiple receptors for dopamine. Nature. 277:93-6.
730	Review.
731	Kestell GR, Anderson RL, Clarke JN, Haberberger RV, Gibbins IL (2015) Primary
732	afferent neurons containing calcitonin gene-related peptide but not substance P in forepaw skin,
733	dorsal root ganglia, and spinal cord of mice. J. Comp. Neurol. 523:2555-69.
734	Kiang NY, Rho JM, Northrop CC, Liberman MC, Ryugo DK (1982) Hair-cell
735	innervation by spiral ganglion cells in adult cats. Science. 217:175-7.
736	Krause JE, Chirgwin M, Carter MS, Xu ZS, Hershey AD (1987) Three rat
737	preprotachykinin mRNAs encode the neuropeptides substance P and neurokinin A. Proc Natl
738	Acad Sci. 84:881-5.
739	Kujawa SG, Liberman MC (2009) Adding insult to injury: cochlear nerve degeneration
740	after "temporary" noise-induced hearing loss. J Neurosci. 29:14077-14085.
741	Lahne M, Gale JE (2008) Damage-induced activation of ERK1/2 in cochlear supporting
742	cells is a hair cell death-promoting signal that depends on extracellular ATP and calcium. J
743	Neurosci. 28:4918-4928.
744	Lahne M, Gale JE. (2010) Damage-induced cell-cell communication in different cochlear
745	cell types via two distinct ATP-dependent Ca waves. Purinergic Signal. 6:189-200.

Lallemend F, Lefebvre PP, Hans G, Rigo JM, Van de Water TR, Moonen G, Malgrange

Keenan WT, Dubin AE, Lewin GR, Patapoutian A (2018) The mechanosensitive ion channel

770 10:eaat9897. 771 Nario K, Kitano I, Mori N, Matsunaga T (1995) The action of substance P methyl ester 772 on cochlear potentials in the guinea pig. Eur Arch Otorhinolaryngol. 252:42-7. 773 Pagani M, Albisetti GW, Sivakumar N, Wildner H, Santello M, Johannssen HC, 774 Zeilhofer HU (2019) How gastrin-releasing peptide opens the spinal gate for itch. Neuron. 775 103:102-117. 776 Perkins RE, Morest DK (1975) A study of cochlear innervation patterns in cats and rats 777 with the Golgi method and Nomarkski optics. J. Comp. Neurol. 163:129-58. 778 Pienkowski M, Tyler RS, Roncancio ER, Jun HJ, Brozoski T, Dauman N, Coelho CB, 779 Andersson G, Keiner AJ, Cacace AT, Martin N, Moore BCJ (2014) A review of hyperacusis and 780 future direction: part II. Measurement, mechanisms, and treatment. Am. J. Audiol. 23:420-36. 781 Robertson D (1984) Horseradish peroxidase injection of physiologically characterized 782 afferent and efferent neurones in the guinea pig spiral ganglion. Hearing Res. 15:113-21. 783 Robertson D, Sellick PM, Patuzzi R (1999) The continuing search for outer hair cell 784 afferents in the guinea pig spiral ganglion. Hearing Research. 136:151-158. 785 Shrestha BR, Chia C, Wu L, Kujawa SG, Liberman MC, Goodrich LV (2018) Sensory neuron diversity in the inner ear is shaped by activity. Cell. 174:1229-1246. 786 Sirko P, Gale JE, Ashmore JF (2019) Intercellular Ca²⁺signalling in the adult mouse 787 788 cochlea. J Physiol. 597:3030-317.

Piezo2 mediates sensitivity to mechanical pain in mice. Science Translational Medicine.

789 Sleigh JN, Weir GA, Schiavo G (2016) A simple, step-by-step dissection protocol for the

rapid isolation of mouse dorsal root ganglia. BMC Res Notes. 9:82

fibers in the spared nerve injury mouse model. Molecular Pain. 9:61. Smith CA (1975) Innervation of the cochlea of the guinea pig by use of the Golgi stain. Ann Otol Rhinol Laryngol. 84:443-58. Stamataki S, Francis HW, Lehar M, May BJ, Ryugo DK (2006) Synaptic alterations at inner hair cells precede spiral ganglion cell loss in aging C57BL/6J mice. Hear Res. 221:104-Sun W, Ding DL, Wang P, Sun J, Jin X, Salvi RJ (2004) Substance P inhibits potassium and calcium currents in inner ear spiral ganglion neurons. Brain Research. 1012:82-92. Talagas M, Lebonvallet N, Berthod F, Misery L (2020) Lifting the veil on the keratinocyte contribution to cutaneous nociception. Protein Cell. 11:239-250. Tritsch NX, Eunyoung Y, Gale JE, Glowatzki E, Bergles DE (2007) The origin of spontaneous activity in the developing auditory system. Nature. 450:50-55. Tritsch NX, Zhang Y, Ellis-Davies G, Bergles DE (2010) ATP-induced morphological changes in supporting cells of the developing cochlea. Purinergic Signalling. 6:155-166. Tyler RS, Pienkowski M, Roncancio ER, Jun HJ, Brozoski T, Dauman N, Andersson G, Keiner AJ, Cacace AT, Martin N, Moore BCJ (2014) A review of hyperacusis and future direction: part I. Definitions and manifestations. Am. J. Audiol. 23:402-19. Vyas P, Wu JS, Zimmerman A, Fuchs PA, Glowatzki E (2017) Tyrosine Hydroxylase expression in type II cochlear afferents in mice. JARO.18:139-151. Vyas P, Wu JS, Jimenez A, Glowatzki E, Fuchs PA (2019) Characterization of transgenic mouse lines for labeling type I and type II afferent neurons in the cochlea. Scientific reports.

Smith AK, O'Hara CL, Stucky CL (2013) Mechanical sensitization of cutaneous sensory

814 Weissner W, Winterson BJ, Stuart-Tilley A, Devor M, Bove GM (2006) Time course of 815 substance P expression in dorsal root ganglia following complete spinal nerve transection. J 816 Comp Neurol. 497:78-87. 817 Weisz CJC, Glowatzki E, Fuchs PA (2009) The postsynaptic function of type II cochlear 818 afferents. Nature. 461:1126-9. 819 Weisz CJC, Glowatzki E, Fuchs PA (2014) Excitability of type II cochlear afferents. J 820 Neurosci. 34:2365-73. 821 Weisz CJC, Lehar M, Hiel H, Glowatzki E, Fuchs PA (2012) Synaptic transfer from 822 outer hair cells to type II afferent fibers in the rat cochlea. J Neurosci. 32:9528-9536. 823 Weisz CJC, Williams S-PG, Eckard CS, Divito CB, Ferreira DW, Fantetti KN, Dettwyler SA, Cai H-M, Rubio ME, Kandler K, Seal RP (2021) Outer hair cell glutamate signaling through 824 825 type II spiral ganglion afferents activates neurons in the cochlear nucleus in response to 826 nondamaging sounds. J Neurosci. 41:2930-2943. 827 Wood MB, Nowak N, Mull K, Goldring A, Lehar M, Fuchs PA (2021) Acoustic trauma 828 increases ribbon number and size in outer hair cells of the mouse cochlea. JARO. 22:19-31. 829 Wu JS, Vyas P, Glowatzki E, Fuchs PA (2018) Opposing expression gradients of 830 calcitonin-related polypeptide alpha (Calca/Cgrpa) and tyrosine hydroxylase (Th) in type II 831 afferent neurons of the mouse cochlea. J Comp Neurol. 526:425-438. 832 Wu JS, Yi E, Manca M, Javaid H, Lauer AM, Glowatzki E (2020) Sound exposure 833 dynamically induces dopamine synthesis in cholinergic LOC efferents for feedback to auditory 834 nerve fibers. eLife. 9:e52419. 835 836

837 FIGURE LEGENDS

838

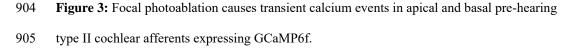
Figure 1: Type II-afferent-associated genes drive GCaMP6f expression. 839 A. Image taken through a dissecting microscope of an excised, otic capsule preparation with 840 access to the apical turn. "a" indicates the location of the tip of the apical turn of the cochlear epithelium. B. Maximum intensity projection image of a whole mount preparation of the apical 841 turn of a Th^{2A-CreER};GCaMP6f mouse. The GFP expression associated with GCaMP6f expression 842 has been pseudo-colored cyan. C. Maximum intensity projection image of Th^{2A-CreER};GCaMP6f 843 844 expression in the peripheral dendrites of apical type II afferent neurons. GCaMP6F expressing 845 type IIafferentss are labeled in cyan (c1); the pan-neuronal marker Tuj1 is labeled in yellow (c2). The overlay with Tuj1 (c3 -green) shows Th^{2A-CreER};GCaMP6f expression in neurons in the OHC 846 847 region of the organ of Corti as indicated by the white circles. **D**. Image taken through a 848 dissecting microscope of an excised, otic capsule preparation with access to the basal turn. "b" 849 indicated the end of the basal turn of the cochlea. E. Maximum intensity projection image of a whole mount preparation of the basal turn of a Drd2^{Cre};GCaMP6f mouse. The GFP expression 850 851 associated with GCaMP6f expression is shown in green. F. Maximum intensity projection image of Drd2^{Cre};GCaMP6f expression in the somata and peripheral dendrites of basal type II afferent 852 853 neurons. Two 40x magnification images were stitched using the pairwise stitching plugin in 854 ImageJ to visualize the path of the neuron from soma to organ of Corti. Hair cell location is 855 indicated by white circles. G. Diagram showing the tonotopic expression patterns of Th (cyan) 856 and Drd2 (green) in the cochlea. H. Diagram showing the morphology of type II afferent 857 neurons in the middle turn of the cochlea. Type II morphology includes a dendritic arbor with a characteristic 90° turn toward the base of the cochlea. Th (cyan); Drd2 (green) I. Diagram of the 858

859	morphological differences between type I afferent neurons (yellow) and type II afferent neurons
860	(Drd2-expressing, green; Th-expressing, cyan) in the organ of Corti.
861	
862	
863	
864	
865	
866	
867	
868	
869	
870	
871	
872	
873	
874	
875	
876	
877	
878	
879	
880	
881	

A. Diagram of typical photoablation experiment of a Th^{2A-CreER};GCaMP6f animal with 883 884 three timepoints illustrated. A timeline of the experimental recording is to the right (not 885 to scale). The timeline is broken after video frame 375 (30 seconds into the recording) to 886 indicate the time when the laser is active, and no imaging occurred. The imaging begins 887 again at frame 376. a1-2. Image still of raw footage from frame 188 (15 seconds into the 888 recording) and a standard deviation projection image of the first 375 frames corresponding 889 to the first 30 seconds of the recording before photoablation. a3-4. Image still of raw 890 footage from frame 563 (15s after photoablation ends), and a standard deviation projection 891 image of frames 376-1125 corresponding to the 30 seconds following the photablation 892 ending. a5. Still of raw footage from frame 3563 (15s before the end of the recording). 893 a6. A standard deviation projection image of frames 894 3375-3750 corresponding to the last 30 seconds of the recording. B. Standard deviation 895 image of the all frames from the recording shown in A (b1), the same image with hand-896 drawn regions of interest around neurons and the site of damage (b2). Arrow points to 897 $\Delta F/F$ traces of a region of interest (b4). Gray portion of the graph represents the area 898 between three standard deviations of the first 375 frames and last 375 frames of the 899 trace. The trace's peak rises above and returns to a steady state below the gray area. This 900 criterion marks the trace from the region of interest as responsive. Responsive regions of 901 interest are outlined with yellow (b3). Red lines above graphs indicate when the laser is 902 on; since no imaging is occurring the trace is set to 0 at this time. Scale bars = $25 \mu m$.

903

Figure 2: Experimental design for testing type II afferent response to acute damage.



A. A standard deviation image of a pre-hearing Th^{2A-CreER};GCaMP6f mouse cochlea after focal 906 907 ablation of OHCs with 1000 iterations of 100% laser power. B. Same image as A. but with hand 908 drawn regions of interest overlaid. Responsive regions of interest are outlined in yellow. Scale 909 bars = 25 μ m. C. Δ F/F traces of responsive ROIs from B. Δ F/F at time of photoablation and until 910 imaging restarts is set to 0. Red line above graph indicates the time the laser was on. The black 911 line above the graph indicates the average response duration for all traces shown. D. Averaged and scaled $\Delta F/F$ traces from each pre-hearing $Th^{2A-CreER}$; GCaMP6f with different shades of blue 912 913 per animal. Black line within graph is the average of all the animal average traces. $\Delta F/F$ at time 914 of photoablation and until imaging restarts is set to 0. E. A standard deviation image of a prehearing Drd2^{Cre};GCaMP6f mouse cochlea after focal ablation of OHCs with 1000 iterations of 915 916 100% laser power with hand drawn regions of interest overlaid. Responsive regions of interest 917 are outlined with yellow. Scale bars = 25 μ m. **F**. Δ F/F traces of responsive ROIs from E. Δ F/F at 918 time of photoablation and until imaging restarts is set to 0. G. Averaged and scaled $\Delta F/F$ traces from each pre-hearing Drd2^{Cre};GCaMP6f with different shades of green per animal. Black line 919 920 within graph is the average of all the animal average traces. $\Delta F/F$ at time of photoablation and 921 until imaging restarts is set to 0.

- 922
- 923
- 924
- 925
- 926

927	Figure 4: ATP blockade prevents the response of distant type II cochlear afferent fibers.
928	A. A standard deviation projection image of a pre-hearing $Drd2^{Cre}$; GCaMP6f with 100 μ M
929	PPADS in the extracellular solution with hand drawn ROIs. Yellow outlined ROIs represent
930	responsive ROIs. Scale bar = 25 μ m. B . Δ F/F traces of the transiently responding ROIs in A.
931	Δ F/F at time of photoablation and until imaging restarts is set to 0. Red line above graph
932	indicates the time the laser was on. The black line above the graph indicates the average response
933	duration for all traces shown. C. Averaged and scaled $\Delta F/F$ traces of responses from each pre-
934	hearing $Drd2^{Cre}$; GCaMP6f animal when 100 µM PPADS was in the extracellular solution with
935	green colors representing different Drd2 ^{Cre} ;GCaMP6f animal and blue representing Th ^{2A-}
936	^{CreER} ;GCaMP6f. Black line is the average of all the animal average traces. Δ F/F at time of
937	photoablation and until imaging restarts is set to 0. Red line above graph indicates the time the
938	laser was on. The black line above the graph indicates the average response duration for all
939	traces shown. D . Histogram of the response duration in seconds from the onset of photoablation
940	to the time the response returns within three standard deviations of the steady state from pre-
941	hearing animals with 100 μ M PPADS and without 100 μ M PPADS (CTL) in the extracellular
942	solution. Blue dots represent Th ^{2A-CreER} ;GCaMP6f animals and green dots represent
943	Drd2 ^{Cre} ;GCaMP6f animals. Horizontal bar and vertical line represent average and standard
944	deviation for each group. E. Histogram of the proportion of the area of responding neural ROIs
945	to total area of neural ROIs for recordings from pre-hearing mice in 100 μ M PPADS and without
946	100 µM PPADS (CTL) in the extracellular solution. Blue dots represent Th ^{2A-CreER} ;GCaMP6f
947	animals and green dots represent Drd2 ^{Cre} ;GCaMP6f animals. Horizontal bar and vertical line
948	represent average and standard deviation for each group. $**$, $p = 0.00011$.
949	

951 spontaneously. A. Standard deviation image of a recording from a pre-hearing $Drd2^{Cre}$ animal with no 952 953 GCaMP6f expression. **B**. Same image as A. but during the frames when spontaneous increase in 954 fluorescence occurred. C. Image generated by subtracting B from A. Scale bars = $25 \,\mu m$. 955 Brackets on the side refer to the location of OHCs, IHCs, and Kölliker's organ (KO) in the 956 image. D. Percent of total pixels above an arbitrary threshold from spontaneous events from the 957 recording in A. and B. Black bars represent the time of the images in A. and B. Red bar denotes 958 the time when photoablation occurred. The NGAF deflection immediately following 959 photoablation is disregarded from analysis and is shown as dashed lines. E. Standard deviation image of a recording from a mature Th^{2A-CreER};GCaMP6f animal. F. Same image as E. but during 960 961 the frames when spontaneous increase in fluorescence occurred. G. Image generated by 962 subtracting F. from E. Scale bars = $25 \,\mu$ m. H. Percent of total pixels above an arbitrary threshold

Figure 5: Non-GCaMP6f associated fluorescence (NGAF) is PPADS sensitive and can occur

963 from spontaneous events from the recording in E. and F. Black bars represent the time of the

964 images in A. and B. Red bar denotes the time when photoablation occurred. The NGAF

965 deflection immediately following photoablation is disregarded from analysis and is shown as

966 dashed lines. I-J. (Left) Paired dot and (Right) box and whisker plot of log transformed area

967 under the curve values from paired NGAF recordings before and after the addition of control

968 extracellular solution (I.) or 100 μ M PPADS in the extracellular solution (J.). *, p = 0.0071.

969

950

- 971
- 972

995

973

974	axis and has broad supporting cell expression in the apex.
975	A-B. 5x magnification confocal images of pre-hearing <i>Tac1^{Cre}</i> ; Ai9 mouse apical (A) and basal
976	segments of cochlea. Scale bar = 100 μ m. C-D. 25x magnification confocal images of a pre-
977	hearing Tac1 ^{Cre} ; Ai9 mouse middle section of cochlea spanning the spiral ganglion and organ of
978	Corti (C.) and basal organ of Corti (D.) representing the white boxes in A. and B. respectively.
979	c1 and d1 show the magenta channel alone (anti-tdTomato, i.e. Tac1 ^{Cre} -expressing cells), c2 and
980	d2 show the green channel alone (anti-Tuj1, pan-neuronal marker), and c3 and d3 show the
981	overlay of the two channels. Neurons that show co-localized expression of tdTomato and Tuj1
982	appear white. Scale bar = 25 μ m. E . Histogram of spiral ganglion cell somata count with 10%
983	bins across the tonotopic axis. * = p<0.05., ** = p<0.01. 10% vs 70%: p = 0.044; 10% vs 80% p
984	=0.0033; 10% vs 90%: p =0.020. F . 5x magnification confocal images of a <i>Tac1^{Cre}</i> ; Ai9 dorsal
985	root ganglion. (anti-tdTomato, Tac1 ^{Cre} -expressing cells - magenta; anti-CGRP, C-fiber marker -
986	green) Neurons that show co-localized expression of tdTomato and CGRP appear white. Scale
987	$bar = 100 \ \mu m.$
988	
989	
990	
991	
992	
993	
994	

Figure 6: Expression of GCaMP6f by $Tac1^{Cre}$ driver labels type II afferents along the tonotopic

996	Figure 7: Expression of GCaMP6f by Tac1 ^{Cre} driver reveals type II afferent activity in the base
997	as well as epithelial cell calcium activity in the middle section of the cochlea.
998	A. Standard deviation image of a focal ablation in the middle section of a pre-hearing
999	Tac1 ^{Cre} ;GCaMP6f mouse cochlea with hand drawn ROIs around segments of neurons and
1000	epithelial cells. Scale bar = 25 μ m. Yellow, outlined neuronal segments represent neurons that
1001	significantly respond to the stimulus and orange, outlined epithelial cells represent epithelial
1002	cells that significantly respond. B. $\Delta F/F$ traces from responding epithelial cell ROIs in A. Black
1003	line is the average of all traces. $\Delta F/F$ at time of photoablation and until imaging restarts is set to
1004	0. C. Averaged and scaled $\Delta F/F$ traces for neuronal responses (shades of magenta) from the
1005	middle sections of Tac1 ^{Cre} ;GCaMP6f mice. Black line is the average of the average traces from
1006	each recording. $\Delta F/F$ at time of photoablation and until imaging restarts is set to 0. D . Standard
1007	deviation image of a focal ablation in the basal section of a pre-hearing Tacl ^{Cre} ;GCaMP6f mouse
1008	cochlea with hand drawn ROIs around segments of neurons, epithelial cells, and NGAF activity.
1009	Scale bar = 25 μ m. Yellow outlined neuronal segments represent neurons that significantly
1010	responded to the stimulus, orange outlined ROIs represent epithelial cells that significantly
1011	respond, and dashed, white ROIs represent areas with NGAF activity. E . Average $\Delta F/F$ traces
1012	from responding ROIs in D. Non-GCaMP6f associated fluorescence trace shown in gray,
1013	epithelial cell response in orange, and average neuron response in magenta. $\Delta F/F$ at time of
1014	photoablation and until imaging restarts is set to 0. F. Averaged and scaled $\Delta F/F$ traces for
1015	neuronal responses (shades of magenta) from the basal sections of <i>Tac1^{Cre}</i> ;GCaMP6f mice.
1016	Black line is the average of the average traces from each recording. $\Delta F/F$ at time of
1017	photoablation and until imaging restarts is set to 0. G. Average $\Delta F/F$ traces from responding
1018	ROIs of another prehearing Tac1 ^{Cre} ;GCaMP6f mouse. An example individual epithelial cell

1019	calcium response in yellow, the average epithelial cell response in orange, and average neuron
1020	response in black. $\Delta F/F$ at time of photoablation and until imaging restarts is set to 0. H .
1021	Histogram of the individual response durations from NGAF, epithelial cell and neuron ROIs
1022	across all Tac1 ^{Cre} ;GCaMP6f mice across the cochlea. Triangles represent responses from apical
1023	cochlea sections, diamonds from middle cochlea sections, and squares from basal cochlea
1024	sections. Magenta represents neurons, orange represents epithelial cells, and gray represents
1025	NGAF activity.
1026	
1027	
1028	
1029	
1030	
1031	
1032	
1033	
1034	
1035	
1036	
1037	
1038	
1039	
1040	
1041	

1042 Figure 8: Mature organs of Corti have reduced spread of non-GCaMP6f associated fluorescence1043 (NGAF) and neuronal activation.

Th^{2A-CreER}:GCaMP6f mouse apical cochlea after 1044 A. Standard deviation image of a mature 1045 focal ablation with hand drawn regions of interest around segments of neurons. Yellow, outlined 1046 neuronal segments represent neurons that significantly responded to the stimulus. Scale bar = 251047 μ m. **B**. Δ F/F traces from responding ROIs in A. Δ F/F at time of photoablation and until imaging restarts is set to 0. C. Averaged and scaled traces of all mature Th^{2A-CreER};GCaMP6f and 1048 Drd2^{Cre};GCaMP6f recordings. Black line is the average of the average traces from each 1049 1050 recording. $\Delta F/F$ at time of photoablation and until imaging restarts is set to 0. **D**. Standard deviation image of a mature Tac1^{Cre};GCaMP6f mouse basal cochlea after focal ablation with 1051 1052 hand drawn ROIs around segments of neurons. Yellow, outlined neuronal segments represent 1053 neurons that significantly responded to the stimulus and orange, outlined segment for the 1054 responding epithelial cell. Photoablation occurred within orange outline. Scale bar = $25 \,\mu$ m. E. 1055 Δ F/F traces from responding ROIs in D. Magenta traces represent neural ROIs and orange trace 1056 represents the epithelial ROI. $\Delta F/F$ at time of photoablation and until imaging restarts is set to 0. 1057 F. Averaged and scaled neuronal (magenta), epithelial (orange), and NGAF (gray) traces of all mature $Tac 1^{Cre}$; GCaMP6f recordings. $\Delta F/F$ at time of photoablation and until imaging restarts is 1058 1059 set to 0. G-I. Dot plots of (G.) time of response from the observed peak to the time the response 1060 returns within three standard deviations of the steady state, p = 0.020 and p = 0.041 for the 1061 interaction (mature); (H.) the proportion of area of responding neural ROIs to total area of neural 1062 ROIs, p = 0.0030 and p = 0.0036 for the interaction; and (I.) the log transformed values of the 1063 area under the curve of spontaneous increases in fluorescence from mature mice, p = 0.0346.

1064 Figure 9: Previous acoustic trauma increases the chance for cochlear activity long after an acute1065 damage stimulus has subsided.

A. Average ABR threshold measurements from noise-exposed Th^{2A-CreER};GCaMP6f and 1066 $Drd2^{Cre}$: GCaMP6f mice and their control littermates 1 day before calcium imaging (7 or 21 days 1067 after acoustic trauma). Light evan trace represents control $Th^{2A-CreER}$; GCaMP6f mice, N=8, and 1068 dark cyan represents noise-exposed $Th^{2A-CreER}$; GCaMP6f mice, N = 10. Light green trace 1069 1070 represents control $Drd2^{Cre}$; GCaMP6f mice, N = 4, and dark green represents noise-exposed $Drd2^{Cre}$; GCaMP6f mice, N = 4. Black trace represents 2 control wild-type (C57BL/6J) mice 1071 tested. ****, p = <0.0001. **B**. Δ F/F traces from a representative Th^{2A-CreER};GCaMP6f recording 7 1072 days after noise. Black line is the average of all the ROIs from this recording. $\Delta F/F$ at time of 1073 1074 photoablation and until imaging restarts is set to 0. Red bar denotes time of photoablation. Black 1075 bars denote time windows used to generate images in D. and E. C.Correlation of Neuronal 1076 response rate to NGAF response rate for each group of data. Color indicates genotype. Shape indicates age or condition. Cyan - Th^{2A-CreER};GCaMP6f; Green -Drd2^{Cre};GCaMP6f; Magenta -1077 Tac1^{Cre}:GCaMP6f. Circle - pre-hearing; Triangle - mature; Diamond - Noise-exposed. **D**. 1078 Standard deviation image of a mature 7 days post-noise exposure Th^{2A-CreER};GCaMP6f mouse 1079 1080 apical cochlea 30 seconds after focal ablation for 30 seconds. E. Standard deviation image of the mature 7 days post-noise exposure Th^{2A-CreER};GCaMP6f mouse apical cochlea from C, several 1081 1082 minutes after focal ablation for 30 seconds. Scale bars = $25 \ \mu m$. F. Percent of total pixels above 1083 an arbitrary threshold from spontaneous events from the recording in B-E. Red bar denotes time 1084 of photoablation. Black bars denote time windows used to generate images in D. and E. The 1085 NGAF deflection immediately following photoablation is disregarded from analysis and is 1086 shown as dashed lines. G. Bar plot of the proportion of videos that have neural activity re-

1087	emerge minutes after the photoablation in different conditions. Number of videos with delayed
1088	response over the number of videos with an ablation event displayed in each bar of the bar graph.
1089	CTL - control; NE - noise-exposed, $p = 0.037$. Pre-hearing to noise-exposed, $p = 0.0036$.
1090	
1091	
1092 1093 1094	
1095	
1096	
1097	
1098	
1099	
1100	
1101	
1102	
1103	
1104	
1105	
1106	
1107	
1108	
1109	
1110	

1111 TABLE LEGENDS

- 1112 **Table 1**: Mouse Genotypes and Sources
- 1113 Leftmost column provides the name as used in the text for each mouseline. The center column
- 1114 shows the full mouse line name as found on the Jackson Labs website. The right column shows
- 1115 the source of each of the mouselines.
- 1116 **Table 2**: $Th^{2A-CreER}$ and $Drd2^{Cre}$; GCaMP6f^{fl/fl} Videos
- 1117 Number of videos for *Th*^{2A-CreER} and *Drd2*^{Cre};GCaMP6f mice by category. Individual cells
- 1118 represent the number of videos or mice as defined by the leftmost column for the condition
- 1119 described in the topmost row. Videos for $Th^{2A-CreER}$; GCaMP6f were taken from apical sections of
- 1120 the cochlea whereas videos from *Drd2^{Cre}*;GCaMP6f are from basal sections of the cochlea.
- 1121 Videos recorded when the tissue is bathed in external solution without the presence of PPADS
- 1122 are designated external and ones with PPADS in the bath are designated as PPADS. NGAF
- 1123 refers to non-GCaMP6f associated fluorescence. To calculate the neuronal response rate take the
- 1124 value of # Photoablation with neural response and divide it by the sum of the values for #
- 1125 Photoablation with neural response and # Photoablation without neural response. To calculate
- 1126 the NGAF response rate take the value of # with NGAF and divide it by the sum of the values for
- 1127 # with NGAF and # without NGAF.
- 1128 **Table 3**: *Tac1^{Cre}*;GCaMP6f^{fl/fl} Videos
- 1129 Number of videos for $Tac 1^{Cre}$; GCaMP6f mice by category. Individual cells represent the
- 1130 number of videos or mice as defined by the leftmost column for the condition described in the
- 1131 topmost row. Videos for *Th*^{2A-CreER};GCaMP6f were taken from apical sections of the cochlea
- 1132 whereas videos from *Drd2^{Cre}*; GCaMP6f are from basal sections of the cochlea. Videos recorded
- 1133 when the tissue is bathed in external solution without the presence of PPADS are designated

1134	external and ones with PPADS in the bath are designated as PPADS. NGAF refers to non-
1135	GCaMP6f associated fluorescence. To calculate the neuronal response rate take the value of #
1136	Photoablation with neural response and divide it by the sum of the values for # Photoablation
1137	with neural response and # Photoablation without neural response. To calculate the NGAF
1138	response rate take the value of # with NGAF and divide it by the sum of the values for # with
1139	NGAF and # without NGAF.
1140	Table 4: Noise-exposed and control videos
1141	Number of videos for Th ^{2A-CreER} and Drd2 ^{Cre} ;GCaMP6f noise-exposed mice and their control
1142	littermates by category. Individual cells represent the number of videos or mice as defined by
1143	the leftmost column for the condition described in the topmost row. Videos for Th^{2A}
1144	CreER;GCaMP6f were taken from apical sections of the cochlea whereas videos from
1145	<i>Drd2^{Cre}</i> ;GCaMP6f are from basal sections of the cochlea. Videos recorded when the tissue is
1146	bathed in external solution without the presence of PPADS are designated external and ones with
1147	PPADS in the bath are designated as PPADS. NGAF refers to non-GCaMP6f associated
1148	fluorescence. To calculate the neuronal response rate take the value of # Photoablation with
1149	neural response and divide it by the sum of the values for # Photoablation with neural response
1150	and # Photoablation without neural response. To calculate the NGAF response rate take the value
1151	of # with NGAF and divide it by the sum of the values for # with NGAF and # without NGAF.
1152	To calculate the delayed response rate take the value of # with delayed response and divide it by
1153	the sum of the values for # Photoablation with neural response and # Photoablation without
1154	neural response.
1155	

1157 MULTIMEDIA LEGENDS

1158 Video 1: Photoablation causes NGAF responses in an animal without GCaMP6f fluorescence 1159 Video created from images taken every second before and after a photoablation in a prehearing animal with no GCaMP6f expression. Video has been sped up 20x from raw footage. 1160 1161 The word ablation appears for 1 second just after the photoablation occurs in the top left corner. 1162 Before the photoablation, slight fluorescence changes are seen in the area of the greater epithelial 1163 region corresponding to crenation events. After photoablation, NGAF is observed in the OHC 1164 region. 1165 Video 2: Neuronal and Epithelial cells respond to photoablation in the middle turn of a Tac1^{Cre};GCaMP6F animal. 1166 1167 Video created from images taken every 80 milliseconds before and after a photoablation. 1168 Video has been sped up 20x from raw footage. The word ablation appears in the top left corner 1169 of the video frame for 4 seconds after the photablation event occurs. Neurons and epithelial cells 1170 increase in fluorescence intensity after the photoablation. **Video 3**: Noise exposure causes delayed NGAF and neuronal responses in an adult Th^{2A-} 1171 CreER;GCaMP6f mouse. 1172

1173 Video created from images taken every 80 milliseconds before and after a photoablation 1174 in an adult $Th^{2A-CreER}$;GCaMP6f mouse 7 days after noise exposure. Video has been sped up 20x 1175 from raw footage. The word ablation appears in the top left corner of the video frame for 2 1176 seconds after the photablation event occurs. Several minutes after photoablation (here at the 20 1177 sec mark) neurons and epithelial cells show a delayed increase in fluorescence around the site of 1178 damage.

1179

1181 Table 1: Mouse Genotypes and Sources

Name	Genotype	Source		
Th ^{2A-CreER}		Abraira et al., 2017		
Drd2 ^{Cre}	B6.FVB(Cg)-Tg(Drd2-cre)ER44Gsat/Mmucd	RRID:MMRRC_032108- UCD		
Tac1 ^{Cre}	B6;129S- <i>Tac1^{tm1.1(cre)Hze/}</i> J	IMSR Cat# JAX:021877, RRID:IMSR_JAX:021877		
GCAMP6f ^{fl/fl}	C57BL/6N-Gt(ROSA)26Sor ^{tm1(CAG-GCaMP6f)} Khakh /J	IMSR Cat# JAX:029626, RRID:IMSR_JAX:029626		
Ai9	B6.Cg-Gt(ROSA)26Sor ^{tm9(CAG-tdTomato)Hze} /J	IMSR Cat# JAX:007909, RRID:IMSR_JAX:007909		

Table 2: *Th*^{2A-CreER} and *Drd*2^{Cre};GCaMP6F^{fl/fl}Videos

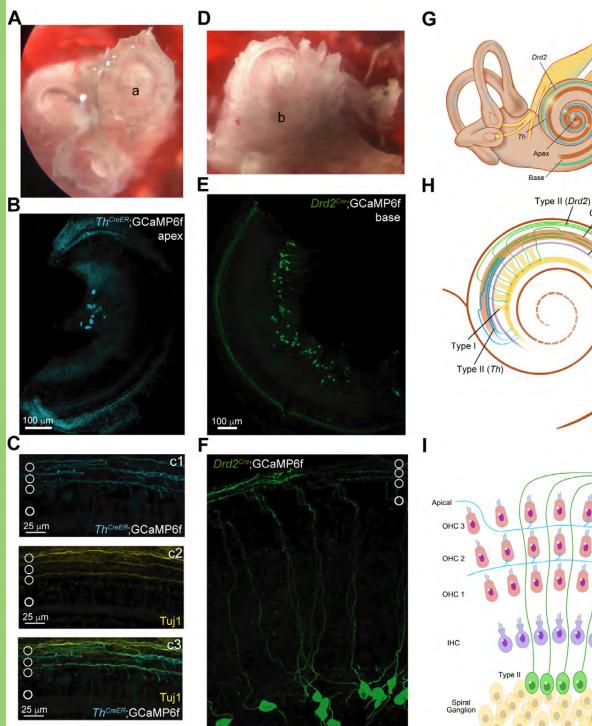
	Pre- hearing	Mature	<i>Th</i> (Apex)	Drd2 (Base)	External	PPADS	Total
Total number of videos (#)	117	144	109	152	204	57	261
# with neurons in view	100	116	90	126	173	43	216
Total number of mice	21	24	18	27	45	23	45
Number of mice with neurons in view	20	23	18	25	43	23	43
# Photoablation with neural response	26	9	11	24	26	9	35
# Photoablation without neural response	19	34	24	29	39	14	53
# Photoablation with no damage	11	34	15	30	40	5	45
# with NGAF	73	51	48	76	97	27	124
# without NGAF	44	93	61	76	107	30	137

Table 3: Tac1^{Cre};GCaMP6f^{fl/fl} Videos

	Pre- hearing	Mature	Apical	Middle	Basal	External	PPADS	Total
Total number of videos (#)	36	38	14	50	10	58	16	74
Total number of mice	6	6	9	10	6	12	8	12
# Photoablation with response	14	8	3	14	5	19	3	22
# Photoablation without neural response	6	8	2	11	1	7	7	14
# Photoablation no damage	4	9	2	9	2	12	1	13
Epithelial cell response	24	4	11	14	3	23	5	28
# with NGAF	2	13	0	11	4	10	5	15

Table 4: Noise-exposed and control videos

	NE	Control	Th (Apex)	Drd2 (Base)	External	PPADS	Total
Total number of videos (#)	74	79	108	45	127	26	153
# with neurons in view	52	62	89	25	93	21	114
Total number of mice	12	13	18	7	25	14	25
Number of mice with neurons in view	11	12	18	5	25	14	23
# Photoablation with neural response	10	7	17	0	16	1	17
#Photoablation without neural response	21	27	31	17	40	8	48
# Photoablation no damage	4	6	8	2	7	3	10
# with NGAF	37	26	41	22	54	9	63
# without NGAF	37	53	67	23	73	17	90
# with delayed response	16	10	23	3	25	1	26



2<u>5 μm</u>

онс И інс

SG

Basa

Type I

THEPP 0 2021 JHUIAAN

.

